

Functional renormalization group study of the quark-meson model with ω and ρ vector mesons

Mohammed Osman,^{*} Defu Hou,[†] and Wentao Wang[‡]

*Institute of Particle Physics (IOPP) and key laboratory of Quark and lepton physics (MOE),
Central China Normal University, Wuhan 430079, China*

Hui Zhang[§]

*Key Laboratory of Atomic and Subatomic Structure and Quantum Control (MOE),
Guangdong Basic Research Center of Excellence for Structure and Fundamental Interactions of Matter,
Institute of Quantum Matter, South China Normal University, Guangzhou 510006, China
Guangdong-Hong Kong Joint Laboratory of Quantum Matter,
Guangdong Provincial Key Laboratory of Nuclear Science, Southern Nuclear Science Computing Center,
South China Normal University, Guangzhou 510006, China
Physics Department and Center for Exploration of Energy and Matter,
Indiana University, 2401 N Milo B. Sampson Lane, Bloomington, IN 47408, USA.*

(Dated: March 12, 2025)

The functional renormalization group (FRG) is a non-perturbative method that considers quantum and thermal fluctuations. Using the FRG flow equations, the critical region of the two-flavor quark-meson model in a finite isospin chemical potential with omega and rho vector mesons interactions is investigated in this work. We also use the mean-field method to calculate the phase diagram in the chiral limit for comparison. The results show that the influences of the omega meson and rho meson on the phase structure are quite different. The existence of the isospin chemical potential also causes significant changes in the phase structure.

I. INTRODUCTION:

The phase diagram of Quantum Chromodynamics (QCD) is a subject of extensive investigation in both experimental and theoretical physics, gathering considerable interest for its application in understanding the fundamental properties of matter under extreme conditions [1, 2]. Since the initial conjecture by N. Cabibbo and G. Parisi in 1975, our comprehension of the QCD phase diagram and the behavior of strongly interacting matter has advanced significantly [3]. Experimental studies and lattice Monte Carlo simulations have notably enhanced our quantitative understanding of the high-temperature region of the QCD phase diagram. However, exploring the phase diagram at high baryon density presents a more formidable challenge. This difficulty primarily stems from the fermion-sign problem, a well-known obstacle in lattice QCD simulations [4]. The fermion-sign problem causes standard lattice techniques to fail in effectively addressing the behavior of QCD matter at high densities. This limitation necessitates the development of alternative approaches to probe the QCD phase structure in such regimes.

The heavy ion collision (HIC) experiments conducted by the STAR Collaboration at the Relativistic Heavy Ion Collider (RHIC) at Brookhaven National Laboratory [5–7] and by the NA61/SHINE Collaboration at the Su-

per Proton Synchrotron (SPS) at CERN [8, 9] are instrumental in elucidating the properties of the quark-gluon plasma (QGP) and mapping the phase boundary of QCD. These experiments provide critical data on the behavior of matter at extremely high temperatures and densities, shedding light on the early universe conditions just microseconds after the Big Bang. Looking forward, upcoming facilities such as the Nuclotron-based Ion Collider facility (NICA) at the Joint Institute for Nuclear Research [10], the Facility for Antiproton and Ion Research (FAIR) at the GSI Helmholtzzentrum für Schwerionenforschung [11], and the J-PARC Heavy Ion Project at the Japan Proton Accelerator Research Complex (J-PARC) [12] will play pivotal roles in advancing our understanding of nuclear properties and quark matter under extreme conditions. These facilities are expected to employ advanced detection technologies and innovative experimental designs to explore new regimes of temperature, density, and magnetic fields, potentially uncovering novel phases of matter and providing deeper insights into the fundamental forces governing particle interactions.

Model calculations using the Nambu–Jona–Lasinio (NJL) model or the Quark-Meson (QM) model can be substantially refined by extending beyond the conventional Mean Field approximation (MF) [13–21]. A notable approach to surpass the constraints of the MF approximation is the application of the renormalization group to continuous field theories. The Functional Renormalization Group (FRG) stands out as a powerful non-perturbative technique, enabling the incorporation of quantum and thermal fluctuations into a field theory. This method provides a more comprehensive and precise understanding of the system’s behavior, thereby enhanc-

^{*} mhdosmn183@mails.cnu.edu.cn.

[†] houdf@mail.cnu.edu.cn.

[‡] wwt@mails.cnu.edu.cn.

[§] Mr.zhanghui@m.scnu.edu.cn.

ing the predictive power and accuracy of the model. The FRG has emerged as a powerful tool for investigating the QCD phase diagram, particularly when employing chiral effective models that transcend the mean field approximation. Notably, the NJL model [22–25] and the QM model [5, 26–31] have been extensively explored using FRG techniques. These investigations have significantly deepened our insights into the intricate phase structure of QCD, allowing for the incorporation of quantum and thermal fluctuations into the analysis. For a comprehensive understanding of the FRG methodology and its applications, detailed evaluations can be found in Ref. [32]

Typically, the FRG method has been predominantly applied to quark models featuring two flavors, accounting for scalar (σ) and pseudoscalar (π) fluctuations [26, 33, 34]. Moreover, investigations have delved into vector (ρ) and axial vector (a1) fluctuations within the isovector channels [35–37]. However, it's worth noting that, to date, the inclusion of ω and ρ -fluctuations has been primarily confined to Walecka-type models, specifically the nucleon- σ - ω and ρ models. These studies have predominantly centered around nuclear matter, particularly focusing on conditions of low temperature and density [38, 39]. In quark modeling, it is well understood that the mean field exerted by ω and ρ mesons significantly impacts the phase boundary and the critical endpoint's positioning [8, 9, 40]. Therefore, it is imperative to examine the robustness of the mean-field framework to fluctuations in ω and ρ .

In this study, we aim to investigate the influence of ω and ρ vector mesons on the critical endpoint within the 2-flavor QM model. We will comprehensively analyze the interplay between these vectors and their impact on the predicted critical endpoint. Our examination will encompass fluctuations in (σ, π, ω) and ρ fields, allowing us to assess their effects on the phase diagram. In the chiral limit, we anticipate observing a characteristic phase transition behavior: second order at high temperatures and low chemical potentials and first order at low temperatures and high chemical potentials. Additionally, our investigation will explore the existence of a tricritical point, where the second-order phase boundary transitions into a first-order one [27, 41, 42].

This paper is organized as follows:

The 2-flavour quark-meson model, including omega and rho vector mesons interaction, mean-field approximation, and the FRG method, is presented in Sect. **II**. In Sect. **III** the results are discussed as the fluctuation effects and their impact on the phase boundaries and the effect of the vector interactions on the critical point. Finally, in Sect. **IV** the summary is presented.

II. THE QUARK-MESON MODEL WITH ω AND ρ VECTOR MESONS

The Lagrangian of the two-flavors QM model with ω and ρ vector mesons in Minkowski space is

$$\begin{aligned} \mathcal{L} = & \bar{\psi} \left(i\gamma_\mu \partial^\mu + \frac{\mu_I}{2} \gamma_0 \tau_3 + \mu \gamma_0 \right) \psi \\ & - \bar{\psi} [g_s (\sigma + i\gamma_5 \boldsymbol{\tau} \cdot \boldsymbol{\pi}) + \gamma_\mu (g_\omega \omega^\mu + g_\rho \boldsymbol{\tau} \cdot \boldsymbol{\rho}^\mu)] \psi \\ & + \frac{1}{2} \partial_\mu \sigma \partial^\mu \sigma + \frac{1}{2} \partial_\mu \boldsymbol{\pi} \partial^\mu \boldsymbol{\pi} - \frac{1}{4} F_{\mu\nu}^{(\omega)} F^{(\omega)\mu\nu} - \frac{1}{4} \mathbf{R}_{\mu\nu}^{(\rho)} \mathbf{R}^{(\rho)\mu\nu} \\ & - U(\sigma, \boldsymbol{\pi}, \omega_\mu, \boldsymbol{\rho}_\mu) \end{aligned} \quad (1)$$

The field strength tensors of the vector bosons ω_μ and $\boldsymbol{\rho}_\mu$ are generally given as:

$F_{\mu\nu}^{(\omega)} = \partial_\mu \omega_\nu - \partial_\nu \omega_\mu$ and $\mathbf{R}_{\mu\nu}^{(\rho)} = \partial_\mu \boldsymbol{\rho}_\nu - \partial_\nu \boldsymbol{\rho}_\mu - g_\rho \boldsymbol{\rho}_\mu \times \boldsymbol{\rho}_\nu$ respectively. A field ψ is the light two-flavor quark field $= (u, d)^T$. And coupled to isoscalar-scalar (σ) and pion ($\boldsymbol{\pi}$) fields transforming as a four-component field $(\sigma, \boldsymbol{\pi})^T$ under the chiral group. A bold symbol stands for a vector, and $\boldsymbol{\tau} = (\tau_1, \tau_2, \tau_3)$, are the Pauli matrices in isospin space, and introducing isospin chemical potential $\mu_I = \mu_u - \mu_d$. Treated as background fields, only ω_0 and ρ_0^3 are non-vanishing and the non-abelian of $\mathbf{R}_{\mu\nu}^{(\rho)}$ does not contribute in practice. A Hubbard-Stratonovich transformation bosonizes these interactions, introducing effective vector-isoscalar and vector-isovector fields, ω_μ and $\boldsymbol{\rho}_\mu$, respectively. While the fluctuations of the $\boldsymbol{\pi}$ and σ fields will be included non-perturbatively, ω_μ and $\boldsymbol{\rho}_\mu$ will be treated as mean fields. These vector bosons conveniently parametrize unresolved short-distance physics. They are not to be identified with the physical omega and rho mesons. The potential for $\sigma, \boldsymbol{\pi}, \omega_\mu$ and $\boldsymbol{\rho}_\mu$ is

$$\begin{aligned} U(\sigma, \boldsymbol{\pi}, \omega_\mu, \boldsymbol{\rho}_\mu) = & \frac{\lambda}{4} (\sigma^2 + \boldsymbol{\pi}^2 - f_\pi^2)^2 \\ & - \frac{m_\omega^2}{2} \omega_\mu \omega^\mu - \frac{m_\rho^2}{2} \boldsymbol{\rho}_\mu \boldsymbol{\rho}^\mu, \end{aligned} \quad (2)$$

where f_π is the pion decay constant. We will use the value $f_\pi = 93$ MeV, and $m_\omega = m_\rho \sim 1$ GeV. The parameters in our model are g_s, g_ω, g_ρ and λ . The values of these parameters can be different for the MF and FRG calculations when we try to reproduce the same value for quantities such as the constituent quark mass of ~ 300 MeV. As for the value of g_ω, g_ρ and m_ν, m_ρ , in our calculation, they always appear in the form of $g_\omega/m_\omega, g_\rho/m_\rho$, so we will not discuss their values independently.

A. Mean-field approximation

The chiral symmetry is explicitly broken in a vacuum, and the expectation values of the meson fields are $\langle \sigma \rangle = f_\pi$ and $\langle \boldsymbol{\pi} \rangle = 0$. Due to the rotational symmetry, only the zero component of the vector fields ω_μ and $\boldsymbol{\rho}_\mu$ can have an expectation value [43]. Only considering the time component ω_0 and ρ_0^3 of the vector fields ω_μ and $\boldsymbol{\rho}_\mu$, the mean-field potential reads as

$$U_{MF}(\sigma, \omega, \rho) = \frac{\lambda}{4}(\sigma^2 - f_\pi^2)^2 - \frac{m_\omega^2}{2}(\omega_0)^2 - \frac{m_\rho^2}{2}(\rho_0^3)^2. \quad (3)$$

The mean-field effective potential is

$$\Omega_{MF} = \Omega_{\psi\bar{\psi}} + U_{MF}(\sigma, \omega_0, \rho_0^3), \quad (4)$$

with thermal quark and antiquark contributions. μ is the quark chemical potential, T is the temperature, and $\beta = \frac{1}{T}$

$$\begin{aligned} \Omega_{\psi\bar{\psi}} = & -\nu_q \int \frac{d^3\mathbf{p}}{(2\pi)^3} \{E_q \theta(\Lambda_{MF}^2 - \mathbf{p}^2)\} \\ & - \frac{\nu_q}{2} T \int \frac{d^3\mathbf{p}}{(2\pi)^3} \left\{ \ln \left[1 + e^{-\beta(E_q - \mu_{eff}^+)} \right] \right. \\ & + \ln \left[1 + e^{-\beta(E_q + \mu_{eff}^+)} \right] \\ & \left. + \ln \left[1 + e^{-\beta(E_q - \mu_{eff}^-)} \right] + \ln \left[1 + e^{-\beta(E_q + \mu_{eff}^-)} \right] \right\}, \end{aligned} \quad (5)$$

where ν_q is the degeneracy factor $\nu_q = 2(\text{spin}) \times 2$ (flavor) $\times 3$ (color) = 12 and $E_q = \sqrt{p^2 + m_{eff}^2}$. The first term is the fermion vacuum fluctuation. The mean fields of the vector bosons enter the partition function just by shifting the chemical potentials; if we eliminated it, the chiral limit transition would always be of first order [44]. We introduce the effective quark(anti-quark) chemical potential given as:

$$\mu_{eff}^\pm = (\mu - g_\omega \omega_0) \pm \left(\frac{\mu_I}{2} + g_\rho \rho_0^3 \right), \quad (6)$$

The effect of the mean field generates an in-medium quark (anti-quark) mass (effective mass)

$$m_{eff} = g_s \sigma, \quad (7)$$

For a given temperature T and chemical potential μ , the mean-field effective potential and the gap equation for ω_0 and ρ_0^3 can be solving quantum equation of motion for ω_0 and ρ_0^3 :

1. For ω_0

$$\begin{aligned} \omega_0 = & \frac{1}{2} \frac{g_\omega}{m_\omega^2} v_q T \int \frac{d^3\mathbf{p}}{(2\pi)^3} \left[\frac{\partial}{\partial \mu_{eff}^+} \left(\ln \left[1 + e^{-\beta(E_q - \mu_{eff}^+)} \right] \right. \right. \\ & \left. \left. + \ln \left[1 + e^{-\beta(E_q + \mu_{eff}^+)} \right] \right) \right. \\ & \left. + \frac{\partial}{\partial \mu_{eff}^-} \left(\ln \left[1 + e^{-\beta(E_q - \mu_{eff}^-)} \right] + \ln \left[1 + e^{-\beta(E_q + \mu_{eff}^-)} \right] \right) \right] \end{aligned} \quad (8)$$

$$\omega_0 = \frac{1}{2} \frac{g_\omega}{m_\omega^2} [n^+ + n^-], \quad (9)$$

2. For ρ_0^3

$$\begin{aligned} \rho_0^3 = & \frac{1}{2} \frac{g_\rho}{m_\rho^2} v_q T \int \frac{d^3\mathbf{p}}{(2\pi)^3} \left[\frac{\partial}{\partial \mu_{eff}^+} \left(\ln \left[1 + e^{-\beta(E_q - \mu_{eff}^-)} \right] \right. \right. \\ & \left. \left. + \ln \left[1 + e^{-\beta(E_q + \mu_{eff}^-)} \right] \right) \right. \\ & \left. - \frac{\partial}{\partial \mu_{eff}^-} \left(\ln \left[1 + e^{-\beta(E_q - \mu_{eff}^+)} \right] + \ln \left[1 + e^{-\beta(E_q + \mu_{eff}^+)} \right] \right) \right], \end{aligned} \quad (10)$$

$$\rho_0^3 = \frac{1}{2} \frac{g_\rho}{m_\rho^2} [n^- - n^+], \quad (11)$$

and the up-quark and down-quark densities, respectively, are determined by

$$n^+(T, \mu_{eff}^+) = -\frac{\partial}{\partial \mu} \Omega_{\psi\bar{\psi}}(T, \mu_{eff}^+), \quad (12)$$

and down-quark

$$n^-(T, \mu_{eff}^-) = -\frac{\partial}{\partial \mu} \Omega_{\psi\bar{\psi}}(T, \mu_{eff}^-), \quad (13)$$

the vector couplings g_ω and g_ρ and the masses of the ω , ρ fields respectively, are not independent, $g_\omega \omega_0$, $g_\rho \rho_0^3$ are proportional to $(\frac{g_\omega}{m_\omega})^2$, $(\frac{g_\rho}{m_\rho})^2$ respectively. Only their ratio $(\frac{g_\omega}{m_\omega})$, $(\frac{g_\rho}{m_\rho})$ appear in calculations for both MF and FRG.

In our calculation, we follow the choice of Ref. [45] and set the parameters $g_s = 3.3$ and $\lambda = 20$, with which the constituent quark mass in a vacuum is $M_{vac} = g_s f_\pi \simeq 307$ MeV, and the sigma mass is $m_\sigma = \sqrt{2\lambda} f_\pi^2 \simeq 588$ MeV.

Remember that the strength of ω_0 and ρ_0^3 field in MF calculations is proportional to the quark density n . After incorporating the fluctuations, nevertheless, the quark number density is equal to the sum of single particle contribution and contributions from other fluctuations; therefore, such a proportional relationship no longer holds.

In the MF calculation, the self-consistent equation for the ω_0 field is directly related to the sum of the quark densities while the one for the ρ_0^3 field is related to the difference in the quark densities. This means that the ρ_0^3 field is zero for symmetric matter ($\rho_0^3 = 0$), i.e. if considering $\mu_u = \mu_d$. Similar results are produced by the FRG calculation.

Indeed, in Ref. [7], it was demonstrated that disregarding recovery is possible for the MF results. However, the

choice of the non-zero ultraviolet value of the ρ_0^3 vector field, $\rho_{0,\Lambda}^3$, resulting in an explicit isospin breaking interaction and to a non-zero ρ_0^3 field, even for symmetric matter. Indeed, in Ref. [46], non-zero values for $\omega_{0,\Lambda}$ were regarded as their influence on the phase diagram was investigated. Nevertheless, there is no cause to regard an ultraviolet potential with explicit isospin breaking by the ρ_0^3 field.

B. FRG flow equation

The FRG is a powerful non-perturbative method that allows incorporating quantum and thermal fluctuations in a field theory [47] and has been extensively applied to effective QCD models [48–50]. The effective average action Γ_k with a scale k obeys the exact functional flow equation

$$\partial_k \Gamma_k = \frac{1}{2} Tr \left[\frac{\partial_k R_k}{\Gamma_k^{(2)} + R_k} \right], \quad (14)$$

Where $\Gamma_k^{(2)}$ is the second functional derivative of the effective average action with respect to the fields, the trace includes momentum integration as well as traces of overall inner indices. An infrared regulator R_k was introduced to suppress fluctuations at momenta below the scale k . The regulator may assume any functional form because it will only interfere with the arbitrarily chosen path in the theory space between these points. In this investigation, quarks serve as the dynamical fields in the flow equation, σ , and $\boldsymbol{\pi}$, and they affect the effective potential and the size of ω_0 and ρ_0^3 fields. Contrary to vector fields' spatial components, Because it is not coupled to the time derivative, the ω_0 and ρ_0 fields are not dynamical.

Therefore, the value of ω_0 and ρ_0^3 are completely fixed by specifying the values of other fields. At each scale k in the flow equation, we determine the values of ω_0 and ρ_0^3 field by solving the consistency equation for given σ , and $\boldsymbol{\pi}$, so the resultant ω_0 and ρ_0^3 may be written as $(\sigma, \boldsymbol{\pi}, \omega_0, \rho_0^3)$. These ω_0 and ρ_0^3 fields in turn appear in the effective chemical potential for quarks, affecting the dynamical fluctuations in the flow equations. Throughout our study we neglect the flow of all wave-function renormalization factors.

The scale-dependent effective potential can be expressed by replacing the potential U with the scale-dependent one U_k ,

$$\Gamma_k = \int d^4x \mathcal{L} | U \rightarrow U_k, \quad (15)$$

with the Euclidean Lagrangian from Eq.(1), Finite temperatures and chemical potentials are treated within

the Matsubara formalism. The time-component is Wick-rotated, $t \rightarrow -i\tau$ and the imaginary time τ is compactified on a circle with radius $\beta = \frac{1}{T}$, where T is the temperature, for which after introduced $\int d^4x \equiv \int_0^{1/T} dx_0 \int_V d^3x$. Due to the chiral symmetry, the potential U depends on σ and $\boldsymbol{\pi}$ only through the chiral invariant

$$\phi^2 = \sigma^2 + \boldsymbol{\pi}^2. \quad (16)$$

As mentioned, the vector fields ω_0, ρ_0^3 appear here only as mean fields. The complete k -dependence is in the effective potential U_k . In analogy to the mean-field potential, the effective potential has a chirally symmetric piece, U_k^ϕ the explicit chiral symmetry breaking term and the mass terms of the vector bosons:

$$U_k = U_k^\phi + U_k^\omega + U_k^\rho, \quad (17)$$

starting with some ultraviolet (UV) potentials U_Λ as our initial conditions, we integrate fluctuations and obtain the scale-dependent U_k .

The form of U_k^ϕ will be determined without assuming any specific forms, while for the potential of the ω and ρ fields, we use the same form as in Eq. (3):

$$U_k^{\omega,\rho} = -\frac{m_\omega^2}{2} (\omega_{0,k})^2 - \frac{m_\rho^2}{2} (\rho_{0,k}^3)^2, \quad (18)$$

use Wetterich's equation, a regulator function, that respects the interpolating limits of the effective average action, has to be chosen. We employ the so-called optimized or Litim regulator function [51], for bosons and fermions, respectively given by:

$$R_k^B(p) = (k^2 - \mathbf{p}^2) \theta(k^2 - \mathbf{p}^2), \quad (19)$$

$$R_k^F(p) = \begin{pmatrix} 0 & ip_i(\gamma_i^E)^T \\ ip_i\gamma_i^E & 0 \end{pmatrix} \left(\sqrt{\frac{k^2}{p^2} - 1} \theta(k^2 - \mathbf{p}^2) \right) \quad (20)$$

because of the structure of the regulators, the dependence on three-momenta is eliminated, and only integral over theta function remains. The flow equation for the potential U_k^ϕ can be obtained as:

$$\begin{aligned} \partial_k U_k^\phi(T, \mu) = & \frac{k^4}{12\pi^2} \left\{ \frac{3[1 + 2n_B(E_\pi)]}{E_q} + \frac{[1 + 2n_B(E_\sigma)]}{E_\sigma} \right. \\ & - v_q \left[\frac{1 - n_F(E_{q,\mu_{eff}^+}) - n_F(E_q, -\mu_{eff}^-)}{E_q} \right] \\ & \left. - v_q \left[\frac{1 - n_F(E_{q,\mu_{eff}^+}) - n_F(E_q, \mu_{eff}^-)}{E_q} \right] \right\}, \quad (21) \end{aligned}$$

where the effective energies are given by:

$$E_\pi = \sqrt{k^2 + M_\pi^2}, \quad (22)$$

$$E_\sigma = \sqrt{k^2 + M_\sigma^2}, \quad (23)$$

$$E_q = \sqrt{k^2 + M_q^2}, \quad (24)$$

for pion, sigma-meson, and quark, respectively. And the scale-dependent particle masses are:

$$M_q^2 = g^2 \phi^2, \quad (25)$$

$$M_\pi^2 = 2U'_k(\phi^2), \quad (26)$$

$$M_\sigma^2 = 2U'_k(\phi^2) + 4\phi^2 U''_k(\phi^2), \quad (27)$$

and we also defined $U'_k = \frac{\partial U_k}{\partial \phi^2}$.

The effective chemical potential,

$$\mu_{eff}^\pm = (\mu - g_\omega \omega_{0,k}) \pm \left(\frac{\mu_I}{2} + g_\rho \rho_{0,k}^3 \right), \quad (28)$$

depends also on the field $\omega_{0,k}$, $\rho_{0,k}$, and both depend on the scale k . The extended occupation numbers simplify to the usual Fermi-Dirac distribution functions for boson and fermion occupation numbers are:

$$n_B(E) = \frac{1}{e^{\beta E} - 1}, \quad n_F(E, \mu) = \frac{1}{e^{\beta(E-\mu)} + 1}. \quad (29)$$

The flow equation for the effective action, the ω_0, ρ fields must be calculated self-consistently. Therefore, at each momentum scale k [7, 46] we solve the mean-field equation for $\omega_{0,k}$ and $\rho_{0,k}^3$.

$$\begin{aligned} \frac{\partial U_k}{\partial \omega_{0,k}} &= 0, \\ \frac{\partial U_k}{\partial \rho_{0,k}^3} &= 0. \end{aligned} \quad (30)$$

The dependence on $\omega_{0,k}, \rho_{0,k}^3$ appears in the mass term and the fermion loop. The flow equation reads:

1. For $\rho_{0,k}^3$

$$\begin{aligned} \partial_k \rho_{0,k}^3 &= - \frac{g_\rho k^4}{\pi^2 m_\rho^2 E_q} \left\{ \right. \\ &\quad - \frac{\partial}{\partial \mu_{eff}^+} \left(n_F(E_q, \mu_{eff}^+) + n_F(E_q, -\mu_{eff}^+) \right) \\ &\quad \left. + \frac{\partial}{\partial \mu_{eff}^-} \left(n_F(E_q, \mu_{eff}^-) + n_F(E_q, -\mu_{eff}^-) \right) \right\}. \end{aligned} \quad (31)$$

On the right side, the first term of down-quark and the other of up-quark. This equation constitutes our flow equations for the ρ field functions of ϕ .

2. For $\omega_{0,k}$

$$\begin{aligned} \partial_k \omega_{0,k}^3 &= - \frac{g_\omega k^4}{\pi^2 m_\omega^2 E_q} \left\{ \right. \\ &\quad \frac{\partial}{\partial \mu_{eff}^+} \left(n_F(E_q, \mu_{eff}^+) + n_F(E_q, -\mu_{eff}^+) \right) \\ &\quad \left. + \frac{\partial}{\partial \mu_{eff}^-} \left(n_F(E_q, \mu_{eff}^-) + n_F(E_q, -\mu_{eff}^-) \right) \right\}. \end{aligned} \quad (32)$$

This equation constitutes our flow equations for the $\omega_{0,k}$ field functions of ϕ .

Note that the flow equations for ω_0 and ρ_0^3 can be solved for a given ϕ , independently of the potential U_ϕ^k (which only tells us where the minimum of ϕ is).

To understand the behavior of ω_0 and ρ_0^3 , for the moment we ignore the k dependence in μ_{eff} , and carry out the integration over k . Then the resulting expression for ω_0 and ρ_0^3 are some factor times the MF expression for the number density. But unlike the MF case, ω_0 and ρ_0^3 are not directly proportional to the physical number density because the baryon density gets contributions not only from single particles but also fluctuations (see Eq.(36)). Moreover, as we will see in Sec.3 if we include the k dependence in μ_{eff} , the $\omega_{0,k}$ and $\rho_{0,k}^3$ fields at k_{IR} are not even proportional to the single-particle contribution. Therefore, the extrapolation of the MF relation $\omega_0 \sim n$ and $\rho_0 \sim n$ does not work without exception to understand the FRG results.

Finally, the initial conditions for the flow equations must be set up. The UV scale Λ should be sufficiently large in order to take into account the relevant fluctuation effects and small enough to render the description in terms of the model degrees of freedom realistic [52]. In our calculation we follow the choice of Ref. [26], $\Lambda = 500$ MeV. The initial for the potential is

$$U_\Lambda^\phi = \frac{\lambda}{4} \phi^4, \quad (33)$$

and set the parameters $g_s = 3.2$, $\lambda = 8$ with the vacuum effective potential from the FRG computation having the minimum at $\sigma_{vac} \simeq 93$ MeV, which is regarded as f_π . We note that the value of λ , which enforces ϕ to stay near f_π , is considerably smaller than the MF case ($\lambda \sim 20$). If we start with another initial condition with an additional ϕ^2 term to give the mass, we need to readjust λ but obtain qualitatively similar results; in fact, starting with the condition Eq.(33), the scale evolution still generates the ϕ^2 terms, reflecting the universality.

The initial condition for the ω and ρ fields has not been examined in detail, and we simply try.

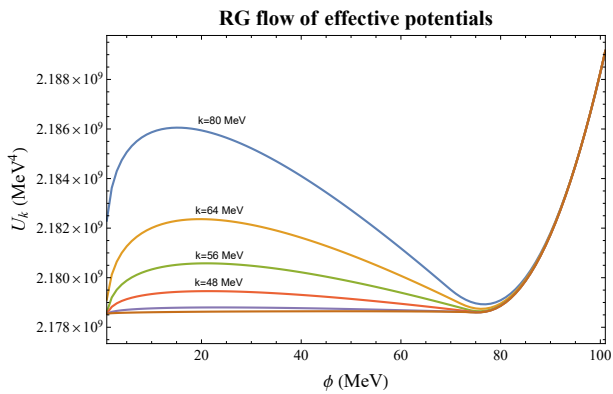


FIG. 1. The evolution of the effective potential with energy scales at $T = 10$ MeV, $\mu = 283$, MeV $\mu_I = 150$ MeV

$$\omega_{0,\Lambda}(\phi) = 0, \rho_{0,\Lambda}^3(\phi) = 0, \quad (34)$$

Later we will also present the result of another different initial condition, but it will turn out that such a modification does not change the main story in this paper.

Assembling all these elements, we calculate the effective potential with the fluctuations integrated to $k_{IR} = 0$. The final step is to find $\Phi = \sigma^*$, which minimizes the effective potential. At the minimum, the effective potential is identified as the thermodynamic potential,

$$\frac{T\Omega(\mu, T)}{V} = \Gamma_{IR=0}(\mu, T, \sigma^*), \quad (35)$$

In practice, it is numerically expensive to reduce the IR cutoff and we typically stop the integration under $k_{IR} \simeq 20$ MeV.

The baryon number density is then obtained by taking the derivative with respect to $\mu_B = N_c \mu$,

$$n_B(\mu, T) = -\frac{1}{N} \frac{\partial \Omega_{k_{IR}=0}(\mu, T, \sigma^*)}{\partial \mu}, \quad (36)$$

The derivative is taken numerically with the interval $\Delta\mu = 0.1$ MeV.

III. RESULTS

A. Effective potential

By numerically solving Eqs. (21), (31), and (32), the results that can be obtained directly are the effective potentials at different energy scales. The evolution of the energy scale ranges from the set 500 MeV to the infrared cutoff less than or equal to 10 MeV. The evolution after the infrared cutoff is considered to remain unchanged

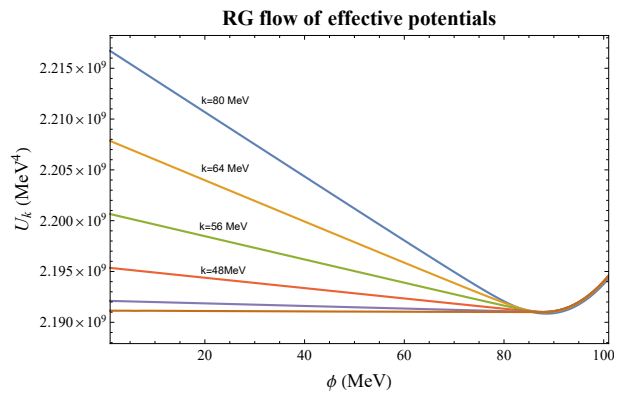


FIG. 2. The evolution of the effective potential with energy scales at $T = 10$ MeV, $\mu = 133.2$, MeV $\mu_I = 550$ MeV

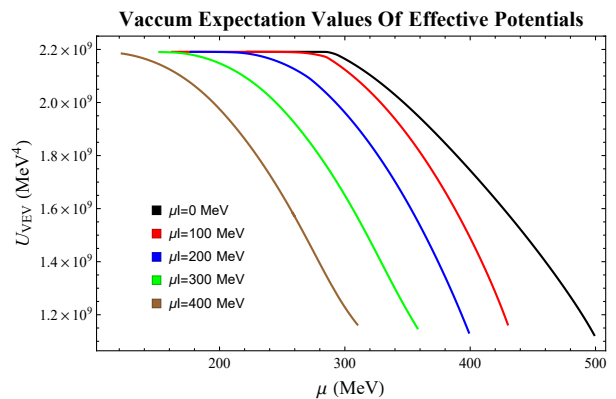


FIG. 3. The vacuum expectation value of the effective potential under different isospin chemical potentials, calculated at $T = 10$ MeV, $g_\omega/m_\omega = g_\rho/m_\rho = 0.006$ [MeV] $^{-1}$. The different colored lines correspond to different isospin chemical potentials.

within the accuracy. Figs. 1 and 2 show the evolution of the effective potential, U_k with energy scale using different isospin chemical potentials, revealing the influence of isospin chemical potential on the effective potential. We compared the cases where the isospin chemical potential is 150 and 550 MeV, respectively.

It can be found that during the process of gradually integrating the fluctuations, the isospin chemical potential significantly changes the value of the effective potential. When focusing on the local characteristics of the effective potential, the influence of fluctuations on the extreme value near $\phi = 0$ is more obvious, but it does not affect the extreme value around $\phi = f_\pi$. On the other hand, as the RG flow evolves with the renormalization time, the effective potential in Fig. 2 flattens at an earlier stage. This implies that isospin asymmetry leads to the inclusion of a greater number of fluctuations in the system at the “early” stage.

Fig. 3 shows the relationship between the vacuum expectation values of corresponding effective potentials,

U_{VEV} , and the chemical potentials under different isospin chemical potentials at low temperatures. Isospin chemical potential introduced in the system does significantly reduce the vacuum expectation value of effective potential at the same temperature and at less quark chemical potential.

B. Chiral condensates

To investigate the peculiar chiral phase transition in the region of low temperature and high chemical potential for isospin asymmetric matter, we can observe the behavior of the order parameter in the low-temperature region under different parameters. This is a typical region where a first-order phase transition should occur, implying that with an increasing quark chemical potential, the order parameter decreases discontinuously from a finite value to a small one, during which the chiral symmetry of the system is restored.

Figs. 4 and 5 illustrate the evolution of chiral condensation with quark chemical potential under the same vector coupling but different isospin chemical potentials. As the isospin chemical potential increases, the quark chemical potential inducing the chiral phase transition gradually decreases. Generally, at the higher temperatures, the initial values of chiral condensation is less than those at low temperatures, and the higher temperatures are closer to the region of second-order phase transition. We note that the increasement of isospin chemical potential also leads to a decreasing initial value of chiral condensation, which corresponding to a reduction in the critical temperature for a system with isospin asymmetry.

Figs. 9 describes the low-temperature behavior of the order parameter under different coupling strengths of rho mesons with finite isospin chemical potentials. Firstly, when the coupling constant is zero (including omega mesons), but there exists finite isospin chemical potential (depicted by the black line in Fig. 6), it is fundamentally different from the matter that lacks both vector coupling and isospin chemical potential (depicted in Fig. 9). The former undergoes a second-order phase transition followed by a first-order phase transition, while the latter undergoes a first-order phase transition followed by a second-order phase transition. In our calculations, we find that this difference brought about by isospin chemical potential is temperature-independent. After accounting for the influence of vector coupling, a system with finite isospin chemical potential may undergo a second-order phase transition followed by a first-order phase transition, while isospin-symmetric matter will certainly undergo a second-order phase transition, followed by a first-order phase transition. On the other hand, in Figs. 6 and Fig. 7, we simultaneously consider the effects of both isospin chemical potential and vector coupling. We find that with an increasing vector coupling, the transition types at smaller quark chemical potential positions con-

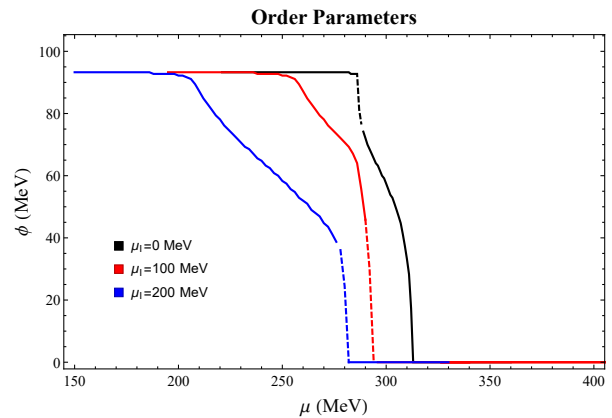


FIG. 4. Chiral condensates as a function of quark chemical potential under different isospin chemical potentials, calculated at $T = 7$ MeV, $g_\omega/m_\omega = g_\rho/m_\rho = 0.006$ [MeV] $^{-1}$. The different colored lines correspond to different isospin chemical potentials.

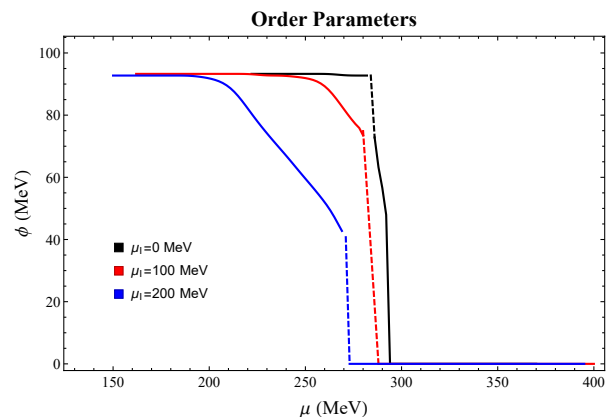


FIG. 5. Chiral condensates as a function of quark chemical potential under different isospin chemical potentials, calculated at $T = 10$ MeV, $g_\omega/m_\omega = g_\rho/m_\rho = 0.006$ [MeV] $^{-1}$. The different colored lines correspond to different isospin chemical potentials.

tinuously changing from second-order to first-order. As we have observed in the results of the effective potential, these phenomena are evidently due to the modification of the vacuum near $\phi = 0$ induced by isospin chemical potential.

C. Baryon number density

Fig. 8 shows the relationship between baryon number density and chemical potential at the same temperature under different isospin chemical potentials. At low isospin chemical potential, there is an obvious first-order phase transition, but when the isospin chemical potential gradually increases, the phase transition type shows a tendency to approach the second-order phase transi-

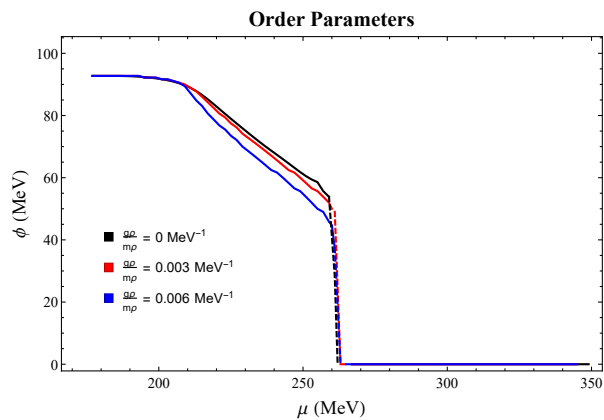


FIG. 6. Chiral condensates as a function of quark chemical potential calculated at $T = 10$ MeV, $\mu_I = 200$ MeV, $g_\omega/m_\omega = 0$ [MeV] $^{-1}$. The plot shows the variation for different g_ρ/m_ρ , different colored lines corresponding to different vector coupling strengths.

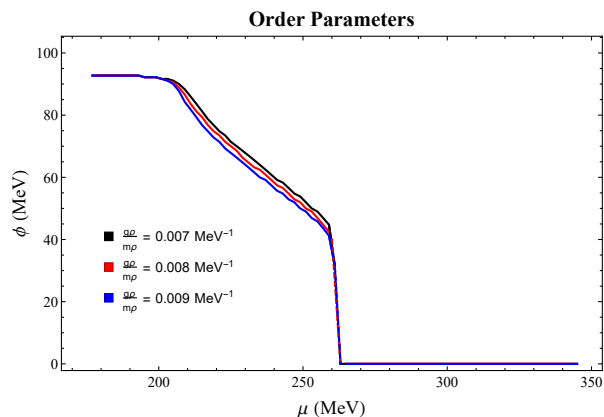


FIG. 7. Chiral condensates as a function of quark chemical potential calculated at $T = 10$ MeV, $\mu_I = 200$ MeV, $g_\omega/m_\omega = 0$ [MeV] $^{-1}$. The plot shows the variation for different g_ρ/m_ρ , different colored lines corresponding to different vector coupling strengths.

tion. In addition, we note that isospin chemical potential enables chiral phase transition to happen in a smaller quark chemical potential. It is assumed that the stronger isospin asymmetry causes the instability of the system, just as the chemical potential plays a role in the interaction.

D. Phase diagram

In this section, we investigate the influence of different isospin chemical potentials on the chiral phase transition in the chiral limit. The FRG equations here we used are the flow equation Eq.(21) for the rho meson given equation Eq.(31) and for the omega meson equation given Eq.(32) for different values of temperature

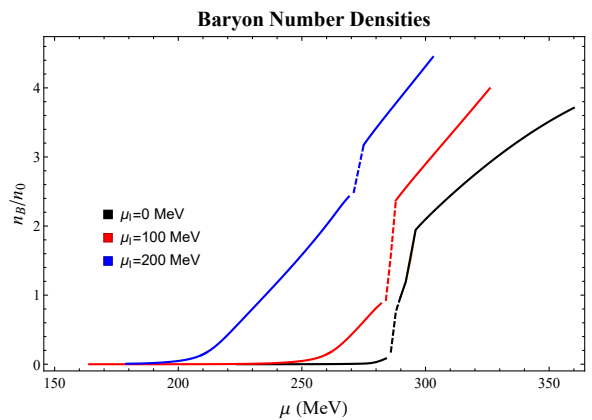


FIG. 8. The change of the baryon number densities with chemical potential when $T = 10$ MeV. The black line is corresponding to $\mu_I = 0$ MeV, the blue line is corresponding to $\mu_I = 200$ MeV, the red line is in $\mu_I = 300$ MeV, the green line is in $\mu_I = 400$ MeV respectively. The baryon number density normalized by the nuclear saturation density $n_0 = 0.16$ fm $^{-3}$.

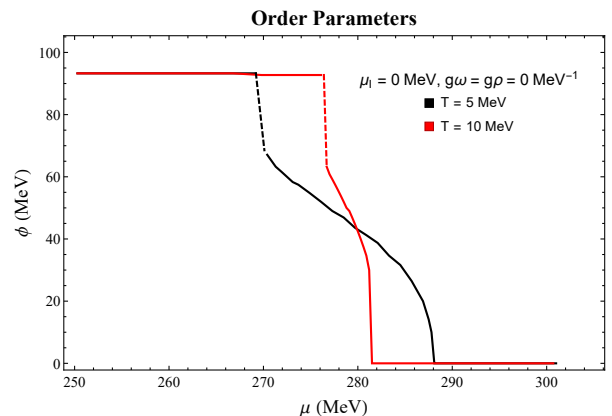


FIG. 9. Chiral condensates as a function of quark chemical potential, calculated when $\mu_I = 0$ MeV and $g_\omega/m_\omega = g_\rho/m_\rho = 0$ [MeV] $^{-1}$. The black and red lines correspond to $T = 5$ MeV and $T = 10$ MeV respectively

and chemical potential. In addition, we also calculate the results obtained by solving the mean-field effective potential equation Eq.(5) using different parameters for qualitative comparison.

Focusing on a fixed temperature, the restoration of chiral symmetry in the hadronic phase requires a higher chemical potential. Figs. 10 and 11 show the chiral phase diagram obtained by different isospin chemical potentials. In contrast to the mean-field method shown in Fig. 11, Fig. 10 shows no “back bending” feature of the functional renormalization group calculation method in the low-temperature region. In this region, as the temperature decreases gradually, the chemical potential required for the phase transition gradually decreases as is most obvious in Ref. [46], while the mean field method shows normal characteristics, the lower the temperature,

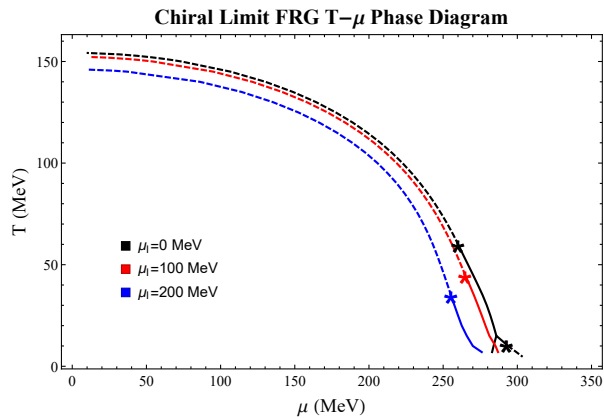


FIG. 10. The FRG $T - \mu$ phase diagram with different μ_I . The solid lines represent the first-order phase transition, and the dashed lines represent the second-order phase transition. The stars show the TCPs. The parameters are set as: $f_\pi = 93$ MeV, $g_s = 3.2$, $\lambda = 8$, the ultraviolet cutoff $\Lambda_{FRG} = 500$ MeV, the coupling constants $g_\omega m_\omega^{-1} = g_\rho m_\rho^{-1} = 0.006$ [MeV] $^{-1}$.

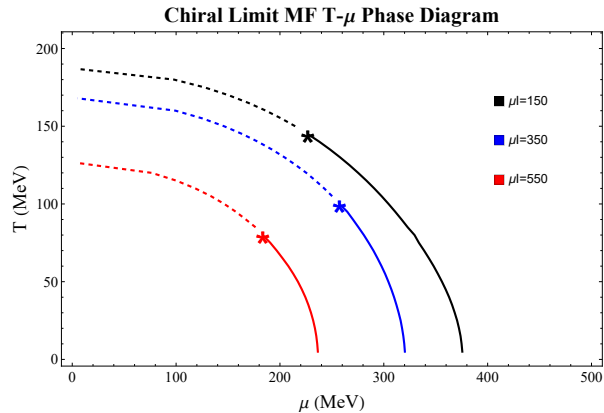


FIG. 11. The mean-field $T - \mu$ phase diagram including vacuum fluctuation ($\Lambda_{MF} = 260$ MeV) for the two-flavor massless QCD with different isospin chemical potentials. Solid lines show the first-order phase transitions, and dashed lines show the second-order phase transition. Dashed lines show the critical points, and the stars show the position of the TCPs.

the chemical potential for the phase transition increases. The “back-bending” feature of the phase diagram obtained by FRG equations has always been a hot topic. The introduction of the chemical potential of isospin and the ρ meson improves this behavior. It is quite understandable that as the isospin chemical potential increases, the fluctuations in the low-temperature region is incorporated into the evolution of the RG flow. This also underscores that the bending effect in the phase diagram is a result of the excessive fluctuation considered in the low-temperature region.

IV. SUMMARY

We have calculated the two flavor quark meson model with omega and rho mesons using the FRG method and the mean-field method to obtain two-phase diagrams and studied the influence of vector mesons and isospin chemical potential on the phase structure of the chiral phase diagram. The main conclusion is divided into two aspects: one is the influence of vector couplings on phase structure, and the other one is the influence of isospin chemical potential on phase structure. we focus on isospin chemical potential influence.

For isospin chemical potential, with the vector coupling strength unchanged, the increase of isospin chemical potential causes the phase boundary to move as a whole to the low temperature and low-density area, and the temperature of TCP also decreases gradually. Differing from only changing the vector coupling as in Ref. [53], the isospin chemical potential also significantly reduces the temperature at which the phase transition occurs at the extremely low chemical potential.

By analyzing the effective potential and baryon number density under different isospin chemical potentials, we believe that the isospin chemical potential contributes to the fluctuations, it changes the vacuum around $\phi = 0$, resulting in corresponding changes in phase structure. Besides considering the combined effects of both types of vector couplings, we have investigated the chiral phase structure of dense isospin asymmetric matter at low temperatures.

Furthermore, the FRG and the MF methods show significant differences in our calculations; That is, the “bending back” effect disappeared in the low-temperature region of the phase diagram except for the non-zero values of the isospin chemical potential in the FRG results. We try to analyze the disappearance of this “back bending”. It can be found that adding rho vector meson will suppress the “bending back” behavior, which is different with Ref. [46]. Increasing the isospin chemical potential will also make the “back bending” phenomenon more obscured. Ref. [49] pointed out that this effect of the QM model is likely due to the regulator adopted by the FRG, which includes too much fluctuation in the evolution process.

ACKNOWLEDGMENTS

We thank Hai-cang Ren and Moran Jia for useful discussions. This work is supported in part by the National Key Research and Development Program of China under Contract No. 2022YFA1604900. This work is also partly supported by the National Natural Science Foundation of China (NSFC) under Grants No. 12435009, and No. 12275104. Hui Zhang acknowledges the financial support from the Guangdong Major Project of Basic and Applied Basic Research (Grant No. 2020B0301030008) and the National Natural Science Foundation of China

(Grant No. 12047523, and 12105107).

-
- [1] P. Braun-Munzinger and J. Wambach, The Phase Diagram of Strongly-Interacting Matter, *Rev. Mod. Phys.* **81**, 1031 (2009), arXiv:0801.4256 [hep-ph].
- [2] F. Rennecke, Vacuum structure of vector mesons in QCD, *Phys. Rev. D* **92**, 076012 (2015), arXiv:1504.03585 [hep-ph].
- [3] J. Eser, M. Grahl, and D. H. Rischke, Functional Renormalization Group Study of the Chiral Phase Transition Including Vector and Axial-vector Mesons, *Phys. Rev. D* **92**, 096008 (2015), arXiv:1508.06928 [hep-ph].
- [4] N. M. Bratovic, T. Hatsuda, and W. Weise, Role of Vector Interaction and Axial Anomaly in the PNJL Modeling of the QCD Phase Diagram, *Phys. Lett. B* **719**, 131 (2013), arXiv:1204.3788 [hep-ph].
- [5] C. Jung, F. Rennecke, R.-A. Tripolt, L. von Smekal, and J. Wambach, In-Medium Spectral Functions of Vector and Axial-Vector Mesons from the Functional Renormalization Group, *Phys. Rev. D* **95**, 036020 (2017), arXiv:1610.08754 [hep-ph].
- [6] M. Drews and W. Weise, Functional renormalization group approach to neutron matter, *Phys. Lett. B* **738**, 187 (2014), arXiv:1404.0882 [nucl-th].
- [7] M. Drews and W. Weise, From asymmetric nuclear matter to neutron stars: a functional renormalization group study, *Phys. Rev. C* **91**, 035802 (2015), arXiv:1412.7655 [nucl-th].
- [8] A. Acharya *et al.* (NA61/SHINE), $K^*(892)^0$ meson production in inelastic p+p interactions at 40 and 80 GeV/c beam momenta measured by NA61/SHINE at the CERN SPS, *Eur. Phys. J. C* **82**, 322 (2022), arXiv:2112.09506 [nucl-ex].
- [9] K. Grebieszkow (NA61/SHINE), New results on fluctuations and correlations from the NA61/SHINE experiment at the CERN SPS, *PoS EPS-HEP2017*, 167 (2017), arXiv:1709.10397 [nucl-ex].
- [10] D. Blaschke, J. Aichelin, E. Bratkovskaya, V. Friese, M. Gazdzicki, J. Randrup, O. Rogachevsky, O. Teryaev, and V. Toneev, Topical issue on Exploring Strongly Interacting Matter at High Densities - NICA White Paper, *Eur. Phys. J. A* **52**, 267 (2016).
- [11] T. Ablyazimov *et al.* (CBM), Challenges in QCD matter physics –The scientific programme of the Compressed Baryonic Matter experiment at FAIR, *Eur. Phys. J. A* **53**, 60 (2017), arXiv:1607.01487 [nucl-ex].
- [12] H. Sako *et al.*, Towards the heavy-ion program at J-PARC, *Nucl. Phys. A* **931**, 1158 (2014).
- [13] E. N. Nikolov, W. Broniowski, C. V. Christov, G. Ripka, and K. Goeke, Meson loops in the Nambu-Jona-Lasinio model, *Nucl. Phys. A* **608**, 411 (1996), arXiv:hep-ph/9602274.
- [14] Y. Nemoto, K. Naito, and M. Oka, Effective potential of O(N) linear sigma model at finite temperature, *Eur. Phys. J. A* **9**, 245 (2000), arXiv:hep-ph/9911431.
- [15] M. Oertel, M. Buballa, and J. Wambach, Meson loop effects in the NJL model at zero and nonzero temperature, *Phys. Atom. Nucl.* **64**, 698 (2001), arXiv:hep-ph/0008131.
- [16] J. Baacke and S. Michalski, O(N) linear sigma model beyond the Hartree approximation at finite temperature, in *6th Workshop on Quantum Field Theory under the Influence of External Conditions (QFEXT03)* (2003) pp. 282–287, arXiv:hep-ph/0312031.
- [17] J. O. Andersen and T. Brauner, Linear sigma model at finite density in the 1/N expansion to next-to-leading order, *Phys. Rev. D* **78**, 014030 (2008), arXiv:0804.4604 [hep-ph].
- [18] D. Müller, M. Buballa, and J. Wambach, The Quark Propagator in the NJL Model in a self-consistent 1/Nc Expansion, *Phys. Rev. D* **81**, 094022 (2010), arXiv:1002.4252 [hep-ph].
- [19] K. Yamazaki and T. Matsui, Quark-Hadron Phase Transition in the PNJL model for interacting quarks, *Nucl. Phys. A* **913**, 19 (2013), arXiv:1212.6165 [hep-ph].
- [20] A. Zacchi and J. Schaffner-Bielich, Effects of Renormalizing the chiral SU(2) Quark-Meson-Model, *Phys. Rev. D* **97**, 074011 (2018), arXiv:1712.01629 [hep-ph].
- [21] R. Câmara Pereira and P. Costa, One-meson-loop NJL model: Effect of collective and noncollective excitations on the quark condensate at finite temperature, *Phys. Rev. D* **101**, 054025 (2020), arXiv:2003.08430 [hep-ph].
- [22] K. Fukushima and J. M. Pawłowski, Magnetic catalysis in hot and dense quark matter and quantum fluctuations, *Phys. Rev. D* **86**, 076013 (2012), arXiv:1203.4330 [hep-ph].
- [23] J. Braun, Fermion Interactions and Universal Behavior in Strongly Interacting Theories, *J. Phys. G* **39**, 033001 (2012), arXiv:1108.4449 [hep-ph].
- [24] K.-I. Aoki, S.-I. Kumamoto, and D. Sato, Weak solution of the non-perturbative renormalization group equation to describe dynamical chiral symmetry breaking, *PTEP* **2014**, 043B05 (2014), arXiv:1403.0174 [hep-th].
- [25] K.-I. Aoki and M. Yamada, The RG flow of Nambu–Jona-Lasinio model at finite temperature and density, *Int. J. Mod. Phys. A* **30**, 1550180 (2015), arXiv:1504.00749 [hep-ph].
- [26] B.-J. Schaefer and J. Wambach, The Phase diagram of the quark meson model, *Nucl. Phys. A* **757**, 479 (2005), arXiv:nucl-th/0403039.
- [27] T. K. Herbst, J. M. Pawłowski, and B.-J. Schaefer, Phase structure and thermodynamics of QCD, *Phys. Rev. D* **88**, 014007 (2013), arXiv:1302.1426 [hep-ph].
- [28] W.-j. Fu and J. M. Pawłowski, Relevance of matter and glue dynamics for baryon number fluctuations, *Phys. Rev. D* **92**, 116006 (2015), arXiv:1508.06504 [hep-ph].
- [29] T. K. Herbst, M. Mitter, J. M. Pawłowski, B.-J. Schaefer, and R. Stiele, Thermodynamics of QCD at vanishing density, *Phys. Lett. B* **731**, 248 (2014), arXiv:1308.3621 [hep-ph].
- [30] R.-A. Tripolt, N. Strodthoff, L. von Smekal, and J. Wambach, Spectral Functions for the Quark-Meson Model Phase Diagram from the Functional Renormalization Group, *Phys. Rev. D* **89**, 034010 (2014), arXiv:1311.0630 [hep-ph].
- [31] J. O. Andersen, W. R. Naylor, and A. Tranberg, Chiral and deconfinement transitions in a magnetic background using the functional renormalization group with

- the Polyakov loop, JHEP **04**, 187, arXiv:1311.2093 [hep-ph].
- [32] N. Dupuis, L. Canet, A. Eichhorn, W. Metzner, J. M. Pawłowski, M. Tissier, and N. Wschebor, The nonperturbative functional renormalization group and its applications, Phys. Rept. **910**, 1 (2021), arXiv:2006.04853 [cond-mat.stat-mech].
- [33] B.-J. Schaefer and J. Wambach, Renormalization group approach towards the QCD phase diagram, Phys. Part. Nucl. **39**, 1025 (2008), arXiv:hep-ph/0611191.
- [34] T. K. Herbst, J. M. Pawłowski, and B.-J. Schaefer, The phase structure of the Polyakov–quark–meson model beyond mean field, Phys. Lett. B **696**, 58 (2011), arXiv:1008.0081 [hep-ph].
- [35] B. Friman, C. Hohne, J. Knoll, S. Leupold, J. Randrup, R. Rapp, and P. Senger, eds., *The CBM physics book: Compressed baryonic matter in laboratory experiments*, Vol. 814 (2011).
- [36] N. Cabibbo and G. Parisi, Exponential Hadronic Spectrum and Quark Liberation, Phys. Lett. B **59**, 67 (1975).
- [37] L. Adamczyk *et al.* (STAR), Beam-Energy Dependence of the Directed Flow of Protons, Antiprotons, and Pions in Au+Au Collisions, Phys. Rev. Lett. **112**, 162301 (2014), arXiv:1401.3043 [nucl-ex].
- [38] L. Adamczyk *et al.* (STAR), Collision Energy Dependence of Moments of Net-Kaon Multiplicity Distributions at RHIC, Phys. Lett. B **785**, 551 (2018), arXiv:1709.00773 [nucl-ex].
- [39] L. Adamczyk *et al.* (STAR), Bulk Properties of the Medium Produced in Relativistic Heavy-Ion Collisions from the Beam Energy Scan Program, Phys. Rev. C **96**, 044904 (2017), arXiv:1701.07065 [nucl-ex].
- [40] P. de Forcrand, Simulating QCD at finite density, PoS **LAT2009**, 010 (2009), arXiv:1005.0539 [hep-lat].
- [41] Y. Lu, Y.-L. Du, Z.-F. Cui, and H.-S. Zong, Critical behaviors near the (tri-)critical end point of QCD within the NJL model, Eur. Phys. J. C **75**, 495 (2015), arXiv:1508.00651 [hep-ph].
- [42] P. Adhikari, J. O. Andersen, and P. Kneschke, Inhomogeneous chiral condensate in the quark-meson model, Phys. Rev. D **96**, 016013 (2017), [Erratum: Phys.Rev.D 98, 099902 (2018)], arXiv:1702.01324 [hep-ph].
- [43] S. Floerchinger and C. Wetterich, Chemical freeze-out in heavy ion collisions at large baryon densities, Nucl. Phys. A **890-891**, 11 (2012), arXiv:1202.1671 [nucl-th].
- [44] V. Skokov, B. Friman, E. Nakano, K. Redlich, and B. J. Schaefer, Vacuum fluctuations and the thermodynamics of chiral models, Phys. Rev. D **82**, 034029 (2010), arXiv:1005.3166 [hep-ph].
- [45] O. Scavenius, A. Mocsy, I. N. Mishustin, and D. H. Rischke, Chiral phase transition within effective models with constituent quarks, Phys. Rev. C **64**, 045202 (2001), arXiv:nucl-th/0007030.
- [46] H. Zhang, D. Hou, T. Kojo, and B. Qin, Functional renormalization group study of the quark-meson model with ω meson, Phys. Rev. D **96**, 114029 (2017), arXiv:1709.05654 [hep-ph].
- [47] J. Berges, N. Tetradis, and C. Wetterich, Nonperturbative renormalization flow in quantum field theory and statistical physics, Phys. Rept. **363**, 223 (2002), arXiv:hep-ph/0005122.
- [48] R.-A. Tripolt, N. Strodthoff, L. von Smekal, and J. Wambach, Spectral functions for the quark-meson model phase diagram from the functional renormalization group, Physical Review D **89**, 034010 (2014).
- [49] R.-A. Tripolt, B.-J. Schaefer, L. von Smekal, and J. Wambach, Low-temperature behavior of the quark-meson model, Phys. Rev. D **97**, 034022 (2018), arXiv:1709.05991 [hep-ph].
- [50] N. Strodthoff and L. von Smekal, Polyakov-Quark-Meson-Diquark Model for two-color QCD, Phys. Lett. B **731**, 350 (2014), arXiv:1306.2897 [hep-ph].
- [51] D. F. Litim, Optimized renormalization group flows, Phys. Rev. D **64**, 105007 (2001), arXiv:hep-th/0103195.
- [52] M. Drews, T. Hell, B. Klein, and W. Weise, Thermodynamic phases and mesonic fluctuations in a chiral nucleon-meson model, Phys. Rev. D **88**, 096011 (2013), arXiv:1308.5596 [hep-ph].
- [53] R. Câmara Pereira, R. Stiele, and P. Costa, Functional renormalization group study of the critical region of the quark-meson model with vector interactions, Eur. Phys. J. C **80**, 712 (2020), arXiv:2003.12829 [hep-ph].